IEEE Robotics and Automation Letters (RAL) paper presented at the
2020 IEEE International Conference on Robotics and Automation (ICRA)
31 May - 31 August, 2020. Paris, France

Distal Hyperextension is Handy: High Range of Motion in Cluttered Environments

Wilson Ruotolo, Rachel Thomasson, Joel Herrera, Alexander Gruebele, and Mark R. Cutkosky
Dept. Mechanical Engineering, Stanford University
Stanford, CA, 94305 USA
wruotolo@stanford.edu

***Abstract*—As robots branch out from the manufacturing sector into the home, there is a pressing need for new technology that can operate in cluttered and unstructured human environments. Loading and unloading a dishwasher serves as a difficult representative challenge for in-home robots, and a new robotic end-effector has been developed for this type of task. The actuation of the fingers is integrated with a bending degree of freedom that is nearly coincident with the proximal joints of the fingers, an arrangement that greatly increases the kinematic workspace in constrained environments. In addition, the distal joints of the fingers are capable of hyperextension (bending backwards), allowing them to pinch a wider range of surface curvatures and angles securely. A third feature of the hand is a palm that combines a granular jamming substrate with suction cups to adhere to wet and slippery objects of varying curvatures. Integration of these features into a single prototype allows the hand to grasp and manipulate dirty dishes reliably and with low gripping forces, as demonstrated in object acquisition and manipulation with less than 10N of applied force.**

***Index Terms*—Manipulation, Under-Actuated Hand, Dexterity Tendon**

I. Introduction

Cleaning the kitchen after eating is a quintessential example of modern inconvenience, making it a perfect candidate for robotic automation. Yet, despite strong incentives, this remains one of the most challenging tasks for robots to complete reliably. Plates and cooking utensils are stacked irregularly on surfaces and in sinks. They may be hard to grasp and difficult to place in confined spaces like the rack of a dishwasher. They may also be dirty or wet, large or small, fragile, and otherwise challenging to grip with a standard arm and gripper. These difficulties combine to make one of the most mundane environments for humans into one of the most pioneering for the next generation of robots. This work explores new design considerations for such environments and implements them in the case of a hand designed for grasping and manipulating dishes.

Supplementary downloadable material is available at http://ieeexplore.ieee.org, provided by the authors. A short video demonstrates key features of the prototype described and it being used for an example manipulation sequence. Toyota Research Institute provided funds to assist the authors with their research but this article solely reflects the opinions and conclusions of its authors and not TRI or any other Toyota entity. This work is also supported by NSF GRFs for W. Ruotolo and R. Thomasson.

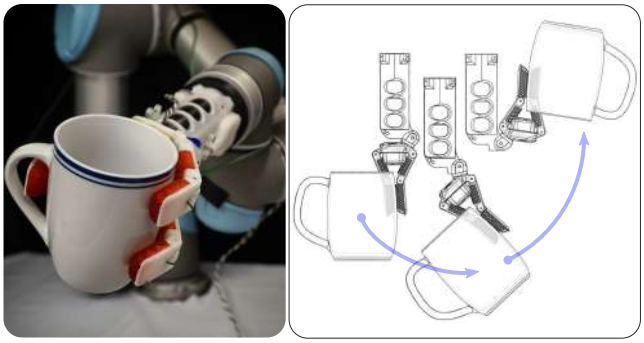

Fig. 1. Left: The prototype hand mounted on UR5 robotic arm demonstrating a traditional enveloping grasp. Right: Diagrammatic representation of a distal hyperextension based pinch on the rim of a cup and hyperextension of the distal bending joint at the wrist allowing increased workspace in cluttered environments.

A. Contributions:

To address the challenges of working in a cluttered and sometimes messy kitchen environment, we present an underactuated hand that allows a robot to reach into confined spaces like dishwashers and refrigerators for placing or extracting items. The hand is also equipped with features to acquire wet and potentially slippery objects and hold them securely.

As shown in Fig. 1, right, the hand includes an additional bending joint near the proximal joints of the fingers, which is actuated using the same tendon system that closes the fingers. This joint has a large range of motion, allowing in-hand rotations to reorient grasped objects without pivoting the robot arm. In addition, tendon forces and joint stiffnesses are tuned so that the distal links bend backwards when grasping thin objects. This hyperextended "power pinch," in combination with a compliant, textured gripping surface, increases security for fingertip grasps, especially with wet and slippery objects. Finally, to acquire challenging objects like inverted plates and bowls, the hand includes a palm with a particle jamming backed suction cup array that can conform to irregularly curved surfaces and adhere to them. Figure 1, left, shows the fabricated prototype hand grasping a cup in a simulated kitchen environment.

B. Related work:

A number of research groups and companies have proposed robotic systems that assist in the kitchen. Apart from ongoing research on vision-based grasping and task planning (e.g. [1]–[3]), demonstrations typically require a highly customized environment (e.g., [4]) and/or customized dishes (e.g. [5]). In general, these efforts have used pre-existing robot arms and hands, rather than customized hardware for the task and environment.

To improve mobility, some anthropomorphic arms and hands include a wrist joint at the base of the palm [6]–[8] however these solutions are generally complex, expensive, and often still cannot match the nearly 180° bending axis sweep achievable by a human hand.

Under-actuated hands have become increasingly popular as a simpler, lighter, and more compact alternative that can still grasp a wide variety of shapes. The design and analysis of compliant, under-actuated hands is covered in detail in [9], [10]. A comprehensive recent review is provided in [11]. The optimization of under-actuated hands to choose joint locations, link lengths, etc. is addressed in [12], [13]. The details of how the fingers close upon objects depend on joint stiffnesses, tendon routing, etc. Among the presented solutions, a "power pinch" [14] is conceptually similar to the distal hyperextension grasps presented in this paper.

Some under-actuated hands can also perform restricted in-hand manipulations. Examples include [15], [16]. The approach taken here allows an in-hand reorientation, using the integral wrist joint.

Objects such as inverted plates and bowls present a particular challenge as hands cannot easily get their fingers beneath them. One solution is to augment a gripper with suction, as used by winning entries in the Amazon Picking Challenge and similar applications [17], [18]. However conventional suction cups with vacuum lines will aspirate water and food particles. An alternative is to use octopus-inspired suckers, as presented in [19]. In [20] suckers are combined with particle jamming to conform to irregular surfaces, however the measured suction is comparatively low on dry surfaces. In this paper we present a new design combining particle jamming and suckers that undergo a relatively large change in volume, which makes them less sensitive to variable surface properties.

II. Design

The design for the wrist and fingers draws inspiration from human manipulation when restricted to a single arm. A wrist was implemented to match the extreme bending mobility of a human appendage, and finger actuation patterns emulate forceful pinches used to exert high torques on small features.

A. Integrated Wrist

1) Configuration Space and Accessibility: For practical reasons it is common for the final axis of a robot to be a roll axis, which makes it easy to rotate objects about an axis roughly perpendicular to the palm. However, rotations about an axis parallel to the palm, or about the axis of an object held in a power wrap grasp [21], require the robot arm to pivot with a large elbow motion. Adding a force/torque sensor at the wrist and a hand with motors housed in its base exacerbates this effect, further separating the fingers from the final bending joint. In contrast, human wrists both roll and bend essentially at the base of the palm, making it comparatively easy to reach into drawers and other confined spaces.

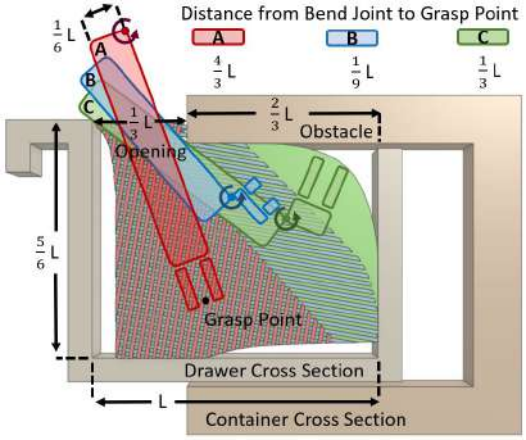

Fig. 2. Visual rendering of the grasp space analysis used to compute a metric of wrist performance. Case A shows a traditional, long robotics wrist length, B shows a wrist that is too short, and C shows a more optimal condition between those two values.

Figure 2 illustrates how a bending axis at the palm increases the effective workspace of the hand when reaching into a drawer; a similar situation pertains in the horizontal plane when reaching into a partially opened cupboard. A long distance between the final bending joint and the fingers decreases the reachable volume by preventing the palm from being able to rotate within such a constrained space (A). Conversely, shifting this bending joint too close allows for a large angular rotation at any point, but prevents the palm from accessing some of the reachable space (B). Preferred values (C) lie between these extremes.

We can quantify this effect with a numerical exploration of the hand's workspace using a parametric variation of the geometry in Fig. 2. First, we define the solution space as a three-dimensional grid of the 2D position of the grasp point and the angle of the fingers about that point, which encodes the freedom in choosing from which direction to grasp an object. Wire frame models of the drawer, shelf obstacle, and hand with the dimensions shown in Fig. 2 are then used to find the achievable subset of the solution space by performing collision checking.

We define workspace coverage as $\gamma = \frac{n}{N} \cdot 100\%$, where N is the total number of points in the gridded workspace and n is the number of points for which there was no collision. Our calculations used a spatial resolution of $\frac{L}{60}$ and an angular resolution of 5° with a 180° range for the bending joint. Figure 3 plots the resulting γ as a 2D solution ("Area") that encodes only positional information, and as a 3D solution ("Volume") that includes the angular component, both as

a function of distance from the wrist to the fingers. Three curves correspond to different ratios of obstacle to opening size, assuming a rectangular workspace, and demonstrate how the impact of bending joint length varies for different workspace volumes.

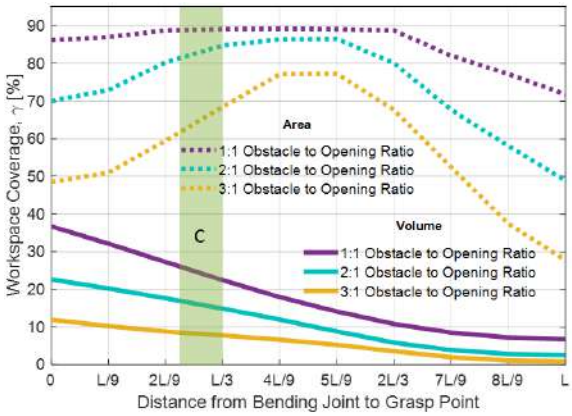

Fig. 3. Using the volumes and areas shown in Fig. 2, the overall efficacy of different segment lengths is shown. Dotted lines represent area only calculations of workspace coverage, whereas solid lines show volume based values. The green band shows workspace coverage values for the prototype produced, which strikes a balance between the area and volume optima.

The volumetric analysis (including grasp angle) in Fig. 3 shows that workspace coverage monotonically decreases as final link length increases. When considering only area coverage, however, there are different peak values depending on environment to hand length ratios. Consequently, the design presented here adopts a compromise in which the distance from the wrist to the expected grasp region is approximately 100mm. This is indicated by the shaded region "C" in Fig. 3 for values of L between 300mm and 400mm, a range which encompasses many standard household drawers.

2) Manipulation and Object Placement: Another consequence of decreasing the distance from the last bending joint to the fingers is that it allows the hand to control the orientation of a grasped object without in-hand manipulation or large arm movements. An example is the case shown in Fig. 1, where the angle of the open face of the cup can be controlled arbitrarily with a small swept volume. This mobility allows the robot arm to pick up bowls and cups and place them in a dish rack (requiring specific release angles) without the risk of a grasp failure during in-hand manipulation and without placing the object down and then regrasping from a different angle. However, there is a cost associated with the integrated wrist: it is difficult to locate sufficiently strong actuators within the hand. Instead, we use remote actuators and tendons (as in the human wrist) which adds an amount of mechanical and control complexity due to interacting torques produced by the associated tendons.

B. Finger Kinematics

Particularly in the case of manipulating fragile objects, it is desirable to reduce the required grasp force for a secure grasp. Numerous solutions for achieving a secure grasp have been presented in the literature on under-actuated hands, however they focus predominantly on achieving enveloping or partially enveloping grasps on convex objects and often, as in [15], do not focus on the significant advantages of plane contact over point contact. Here we adopt a "power pinch" solution often used by humans when grasping thin objects like plates or the rims of cups or bowls. Characterized by distal hyperextension (the tendency of the distal phalange to bend backwards relative to the proximal phalange), this grasp is often used when the object pinched is thinner than the width of the palm and must be acted on with significant torques.

Combined with compliance at the surface contact, distal hyperextension is a way to distribute pressure evenly on convex and concave grasped surfaces. However, in an under-actuated hand it will only occur over a range of grasping angles for certain ratios of joint torques.

Consider the two-phalange loading scenario presented in Fig. 4. For a given proximal joint torque, T_p, there are three major regions of static equilibrium to consider. First, if the torque applied to the distal phalange, T_d, is small or zero, then the normal force applied on the object is effectively a point force situated at the end of the proximal phalange (Fig. 4A). On the opposite end of the continuum, if $T_d = F_d \cdot L_d$, where L_d is the full length of the distal phalange, then the normal force will also be equivalent to a point force, but this time applied at the distal tip of the distal phalange (Fig. 4C). Values beyond this will result in a torque imbalance and curling of the fingertip in the positive θ_d direction. Neither of these conditions is preferable as they both result in a low potential for torque application to the object and a low contact area.

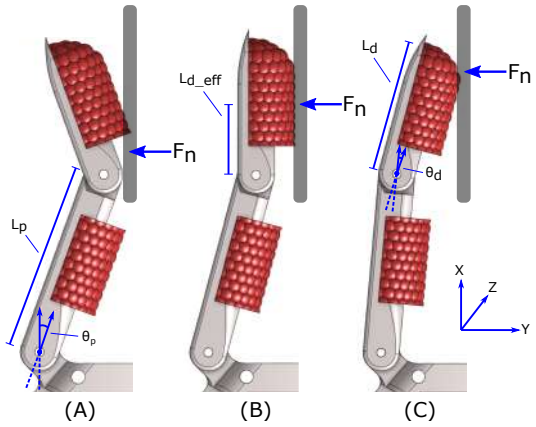

Fig. 4. Conditions for the center of pressure in a "power pinch" contact: A) Insufficient distal torque results proximal contact; B) $T_d = L_d/2 \cdot F_n$ places center of pressure at middle of distal joint; C) High T_d results in over rotation of the distal joint and curling into tip-only contact.

The desired loading scenario lies between these extremes, where the effective length of the distal phalange (i.e. the distance, $L_{d_{eff}}$, from the proximal phalange to the center of pressure of the normal force) equals $L_d/2$ (Fig. 4B). This loading condition distributes the pressure exerted by a compliant fingertip and allows it to exert comparatively large moments across the contact. Further, such a loading condition

improves pull out force because, with soft rubber, the larger area of contact tends to increase the frictional force for a given normal force and the distributed contact also resists twisting moments about the Z-axis defined in Fig. 4.

Under these conditions, T_d and T_p are related to F_n and $L_{d_{eff}}$ as follows.

$$T_p = F_n(L_p \cos\theta_p + L_{d_{eff}} \cos(\theta_p + \theta_d)) \quad (1)$$

$$T_d = F_n(L_{d_{eff}} \cos(\theta_p + \theta_d)) \quad (2)$$

which can be rearranged to solve for $L_{d_{eff}}$ as a function of torques and geometry:

$$L_{d_{eff}} = \frac{T_d L_p \cos\theta_p}{(T_p - T_d)\cos(\theta_p + \theta_d)}. \quad (3)$$

This loading condition ignores frictional effects and assumes small angular deviations, but these approximations are reasonable for the purpose of determining an initial loading scenario as fingers settle on an object and before pull out forces are applied [22], [23]. As a result, a finger design with intentional distal hyperextension should strive to implement joint torques that result in a minimal difference between $L_d/2$ and the right half of Eqn. 3 for as much of the functional range of θ_p and θ_d as possible.

C. Particle Jamming Backed Suction

For reasons discussed in Section I-A, suction is an excellent alternative to anthropomorphic grasps in many situations, but traditional vacuum designs suffer from risk of wet food uptake. On the other hand, compliant, non-aspirated designs must maintain near perfect seals to exert usefully high forces with variations in texture and loading. Further, achieving good seals is difficult on doubly curved surfaces of an unknown geometry. Octopuses meet this challenge by individually aligning each suction cup to match surface angle [19], [24] and distribute force on the suction interface evenly, but this solution requires active sensing and control.

Instead, a similar effect can be accomplished passively if the system is able to switch between compliant and rigid states, making contact while deformable, but then rigidifying before applying load. Such a state transition can be achieved through various mechanisms, but vacuum-controlled particle jamming presents a synergistic solution in this case.

III. Implementation

A. Wrist and Finger Geometry

To realize a prototype hand with a bending joint close to the fingers that is still capable of exerting high torques, the finger and wrist actuation are coupled with a tendon network resulting in two controlled degrees of freedom. A three-finger design was chosen to automatically achieve statically determinant grasps in many situations. Two phalanges per finger are sufficient to achieve both the "power pinch" grasp discussed above and a more traditional enveloping grasp. Proximal and distal phalange lengths were set to 50mm and 35mm respectively, resulting in an overall length similar to human fingers and a ratio that worked well with the rim heights of most dishware. Figure 5 shows the kinematic descriptions as well as the components of the final implementation.

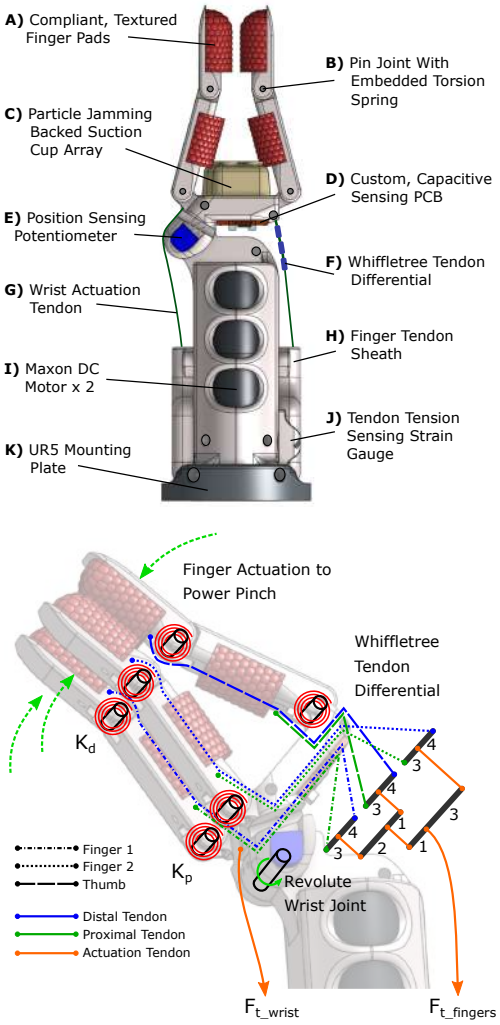

Fig. 5. Top: Hardware components. Bottom: Hand kinematics. Wrist and finger actuation tendons run antagonistically to each other, with the latter propagating its force to the six individual phalanges through a whiffletree differential with segment ratios shown.

With the wrist and finger actuation tendons running antagonistically to each other, it is necessary to regulate their forces such that grasp force is maintained during wrist movement. Two sensors were integrated to provide feedback for this process. A potentiometer is anchored in the wrist joint to provide absolute position information on the angle of the wrist (Fig. 5E), and a strain gauge anchors the finger tendon redirect pulley to provide a force signal (Fig. 5J). These features combine to allow a position value to be specified by the hand controller while the fingers can be actuated with force feedback to achieve a desired grasp strength at any reachable wrist position.

Force ratios at each phalange are, in turn, maintained by the length ratios of a floating whiffletree apparatus mounted between the finger actuator and the phalanges (Fig. 5F). For a symmetric grasp force, the first portion of the whiffletree distributes half of the total force to the thumb and one quarter of the total force to each of the opposing fingers.

The final layer of the whiffletree allocates force to the distal and proximal phalange anchored tendons.

Considering the loading scenario presented in Fig. 4, it is desirable to locate the center of pressure of a pinching finger in the middle of the distal phalange. It is shown in Eqn. 3 that this condition is a function of proximal and distal joint torque as well as joint angle (θ_p and θ_d), thus we calculate T_p and T_d as a function of tendon forces and joint angles and use those values to determine the effective distal phalange length over the functional joint workspace.

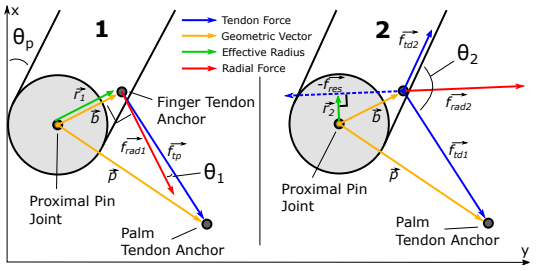

Fig. 6. Vector diagram of resultant tendon tension forces used to calculate effective applied torque at the proximal joint of the proximal phalange. For convenience, the origins of the axes coincide with the centers of rotation of the joints. T_1 represents torque due to proximal tendon and T_2 represents torque due to the distal tendon (both applied to the proximal joint).

Many tendon driven hands route actuation lines around pulleys of a known diameter to control actuation torques, but this method inherently limits the system to certain geometries and prevents the usage of non-linear variations in pulley radii as the fingers close and shift the tendon anchor points closer to or away from the center of rotation. This prototype leaves the distal tendon routed around a pulley when hyperextended, so that radius is consistently defined as a constant r_d, but allows the effective radius and line of force acting on the proximal joint to vary. The geometry is shown in Fig. 6 for the vectors needed to calculate the associated T_p value, which are then defined in equations 4 (vectors for T_1 on the left and vectors for T_2 on the right).

$$
\begin{aligned}
\vec{r_1} = \vec{b} &= Rot(\theta_d) \cdot \begin{bmatrix} 5 \\ 8 \end{bmatrix} \\
\hat{f_{rad}} &= \frac{\begin{bmatrix} r_{1_y} \\ -r_{1_x} \end{bmatrix}}{\left\| \begin{bmatrix} r_{1_y} \\ -r_{1_x} \end{bmatrix} \right\|} \qquad \hat{f_{td_1}} = \hat{f_{tp}} \\
\vec{p} &= \begin{bmatrix} 9.382 \\ -3.5 \end{bmatrix} \qquad \hat{f_{td_2}} = \begin{bmatrix} \cos(\theta_p) \\ \sin(\theta_p) \end{bmatrix} \\
\hat{f_{tp}} &= \frac{\vec{p} - \vec{b}}{\left\| \vec{p} - \vec{b} \right\|} \qquad \theta_2 = \arccos(\hat{f_{td_1}} \cdot \hat{f_{td_2}}) \\
\cos(\theta_1) &= \hat{f_{rad}} \cdot \hat{f_{tp}} \qquad \hat{f_{t_{rad2}}} = \begin{bmatrix} \cos(90 - \theta_p - \theta_2/2) \\ \sin(90 - \theta_p - \theta_2/2) \end{bmatrix} \\
& \qquad \hat{r_2} = \begin{bmatrix} \sin(90 - \theta_p - \theta_2/2) \\ -\cos(90 - \theta_p - \theta_2/2) \end{bmatrix}
\end{aligned}
\tag{4}
$$

Using these values one can calculate r_2 with the following system:

$$
\begin{aligned}
\vec{r_2} &= \vec{b} - \hat{f_{t_{rad2}}} \cdot u \\
\vec{r_2} &= \vec{0} + \hat{r_2} \cdot v
\end{aligned}
\tag{5}
$$

These equations, in turn, allow for the calculation of T_1, T_2, T_p, and T_d, where the last terms of T_p and T_d represent the effect of spring force applied by the embedded torsion springs as a result of angular displacement from their starting value (with some preload to ensure the springs can return the phalanges to their unactuated position):

$$T_1 = F_{prox} \cos(\theta_1) \|\vec{r_1}\| \tag{6}$$
$$T_2 = F_{dist} \cdot 2\cos(\theta_2/2) \cdot r_2 \tag{7}$$
$$T_p = T_1 + T_2 - (180° + \theta_p) k_p \tag{8}$$
$$T_d = F_{dist} \cdot r_d - (45° + \theta_d) k_d \tag{9}$$

Returning to the condition defined in Eqn. 3, this allows for an estimate of the desired force ratio between the proximal and distal tendons. Given that the assumptions made are only valid for a limited angular range and that the "power pinch" grasp is similarly only pertinent for a small subset of grasp configurations, we sweep over $0° \leq \theta_p \leq 45°$ and $-15° \leq \theta_d \leq 15°$ and calculate the effective length of the distal phalange at contact. The result is plotted across the space of those angles for varying total tendon forces as shown in Fig. 7 (left).

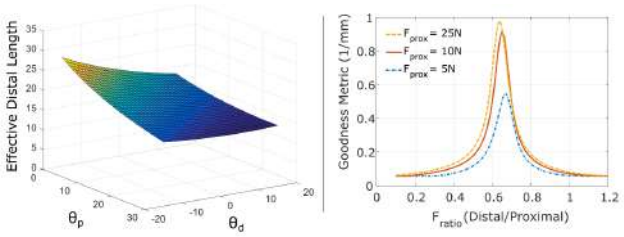

Fig. 7. Left: Example surface plot of effective distal phalange length. Values shown are calculated assuming proximal tendon force of 5 N and a distal/proximal tendon force ratio of 0.69. Right: Metric of goodness plotted as a function of tendon force ratio for three different proximal tension values.

The ideal version of such a plot, where the actuated hand has perfect control of the ratio between the two tendons on each finger would be a flat plane where all values of $L_{d_{eff}} = L_d/2 = 17.5$mm. Given that the hand implemented is limited to a single ratio that is specified by the whiffletree based hardware, it is instead desirable to minimize the average distance of the actual ratio to that ideal plane. Therefore we define a metric by taking the inverse of the average value and plotting it as a function of distal to proximal tendon force ratio. By plotting a range of tendon forces, it can be seen that the ideal value changes only slightly as the spring forces become proportionally less important with increasing applied forces. These curves are shown in Fig. 7 (right).

Thus, to minimize the aforementioned standardized distance and maximize effectiveness across the entire functional range of phalange angles, the initial distal to proximal tendon force ratio is set to 0.69. This improves torque output of a pinch grasp for a given normal force by distributing pressure relatively evenly across a plane of contact; we also hypothesize that this value will improve real area of contact and thereby improve maximum shear force application.

B. Compliant Finger Pads

Compliant pads increase grasp stability by allowing the fingers to conform to the surface of irregularly shaped objects. For a robotic hand operating in a kitchen setting, the texture of these finger pads should have a high coefficient of friction in both dry and wet conditions. Increasing area of contact between the finger pad and grasped object leads to increased friction in both cases. However, while area of contact and surface area are synonymous for the dry case, real contact area in the wet case may be diminished by the presence of a fluid layer between the finger pad and contact surface.

It has been shown that percolation channels allow fluid to drain, increasing real contact area and thus friction in wet conditions [25]. There is a trade-off between nominal surface area and width of these channels. Textures composed of hexagonal pillars were chosen because, for a given gap spacing, tessellated hexagons maximize surface area. It is suspected that pillars with rounded, as opposed to flat, tops may be more successful at expelling fluid into the channels because they contact the surface as a point rather than a plane. When the pillar tops are rounded, the gaps between adjacent pillars can be removed while maintaining small channels. A purely flat tile with no channels results from removing the gaps when pillar tops are flat. Therefore, four categories of texture are considered as shown in Fig. 9.

C. Particle Jamming Backed Suction

To achieve reliable suction with a particle jamming substrate, urethane (Smooth-On Vytaflex30^{TM}) was cast into an outer shell, filled with granular material, and clamped around an outer flange to create a seal (Fig. 8). This implementation uses two features to ensure high suction at each point of contact. First, plastic sucker back supports were fabricated to create particle free chambers into which the outer layer of urethane can collapse under vacuum, approximating the acetabular shape of an octopus sucker. Second, the top surface of each suction cup was allowed to cure open to the air, with the sides wetted to part of the mold. This creates a slim meniscus at the edge of the suction cup that is not in contact with the mold itself, so that upon curing the outer surface of the infundibulum-like component of the suction structure is extremely smooth, very thin, and slightly raised – all conditions desirable for a strong suction effect upon actuation.

IV. Validation

A. Compliant Texture Testing

For each of the four previously mentioned texture categories, three texture sizes were tested. Pillar height was held constant at 1mm and small, medium, and large hexagonal pillars were tested, corresponding to a hexagonal area of πr^2, where $r = 1.75$ mm, 2.5 mm, and 3.25 mm, respectively. For textures with gaps, channel width was fixed at 0.65 mm. Rounded pillars had a radius of curvature of 1.5x the hexagon side length. As flat texture is size independent, this results in ten unique textures.

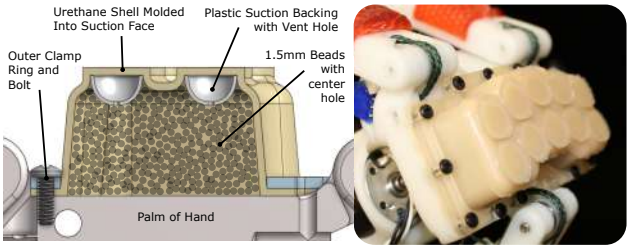

Fig. 8. Left: Section view of the particle jamming backed suction palm schematic. Right: Real prototype mounted on hand. The fully sealed system shown prevents uptake of food particulates and unwanted moisture with its octopus inspired, non-aspirating surface structures.

20mm x 20mm urethane (Smooth-On Vytaflex20^{TM}) pads were mounted on a linear rail system and pressed onto ceramic tiles, both dry and wet, with 20 N of normal force. Shear force was applied until significant movement of the tile was observed. Figure 9 shows the maximum shear force observed for each of the textures, where each data point is the mean of eight trials.

As hypothesized, the purely flat texture performed best in dry conditions, as it had the greatest surface area, but the worst in wet conditions, as there were no channels for fluid to escape. In general, large pillars performed best. When pillars were rounded, textures without gaps outperformed textures with gaps, suggesting that the small channels generated by rounded pillar tops were sufficient for fluid to escape. Therefore, large-scale, rounded topped pillars with no gaps were selected for the compliant finger pads.

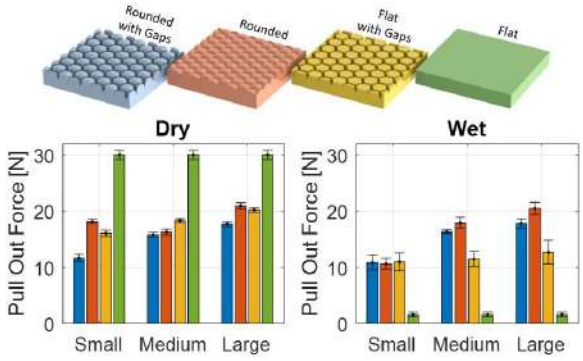

Fig. 9. Above: The categories of texture considered. Below: Compliant finger pad texture testing with colors corresponding to categories above. The bars indicate the maximum pull out force sustained before slipping.

B. Grasp Strength

With a texture defined that is effective on both dry and wet dishes, the next step is to assess overall grasp efficacy in terms of shear force application. A linear stage was equipped with a flat acrylic plate with the edge centered at the height of the palm. The fingers were actuated to grab the acrylic plate in a pinch grasp at low PWM (commanded motor torque) values and the plate was pulled until grasp failure. Tests were repeated with different PWM values of the motor and different distal to proximal tendon force ratios. The resulting pull out forces are plotted in Fig. 10, where each point is an average of five trials.

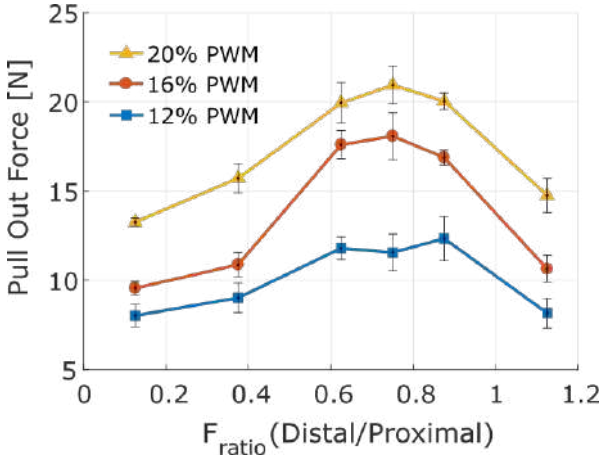

Fig. 10. Pull out data of grasp at different force ratios (distal tendon force/proximal tendon force). Three different total actuation strengths are shown to demonstrate that the optimal force ratio remains relatively constant.

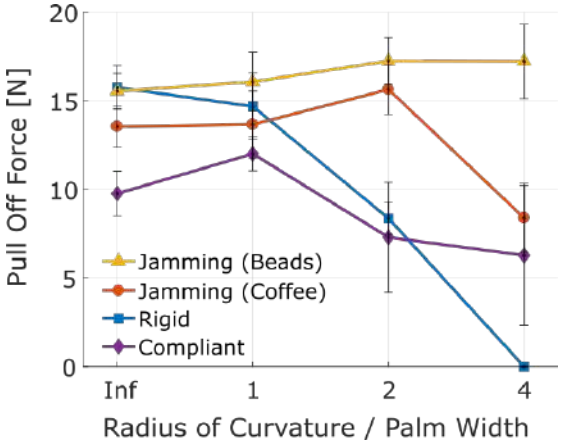

Fig. 11. Pull off force tests of suction cups with various substrate materials. The x-axis shows the radius of curvature of the object on which tests are being performed divided by the palm width to provide information about characteristic length ratios.

Referring back to initial calculations shown in Fig. 7 (right), 0.69 was hypothesized as the best value for the full angular range, but this analysis did not include many minor imperfections such as friction at the pin joints and the capstan friction of the tendon wrapping around internal finger geometry. Pull out tests were performed on the final hand structure, however, and so include such factors.

Nonetheless, it can be seen that the best grasp strength occurred for a range of ratio values from approximately 0.6 to 0.9. Tests at 0.75 gave the best average, but this entire region demonstrated comparable performance within the limits of experimental measurement. This center point agrees quite well with the originally proposed optimal value, and it is logical that frictional effects would spread the range of effective ratio values by making it harder for the finger to roll out of plane contact and into a less desirable configuration (assuming it made good contact in the first place). Thus, we adapted the whiffletree apparatus from these tests to center our value at 0.75 for the final prototype.

C. Load Sharing Across Suction Cups

It was also hypothesized that the particle jamming substrate integrated behind the suction cup array would provide a balance of load sharing and object conformation that outperformed either purely compliant or rigid backings. To confirm this, a pull off test was devised for comparison of potential substrates. A simplified, four panel suction cup of identical sucker geometry was pressed lightly into contact with dishware having a range of surface curvatures. Constant vacuum was then applied and the apparatus was pulled perpendicularly to the surface until attachment failure. Each data point is an average of ten trials. The same urethane shell was used across all trials while different substrate materials were tested. No degradation of shell performance or visible damage was noted, demonstrating durability up to at least 160 load cycles and likely indicating the potential for many more (especially considering that it was allowed to contact many other surfaces before, during, and after testing, adding extra, unmeasured wear).

The results corroborate the original hypothesis, showing that, within the limits of statistical significance, the rigid and particle jamming suction performance is roughly the same for low curvatures, but the rigid performance drops off steeply as curvatures increase while the particle jamming tests do not. Further, the compliant backing (a moderately stiff foam rubber), allows for roughly constant, but generally decreased average performance across the entire range of curvatures.

Two different particle options were compared to show the effects of different granularity levels. The plastic beads were smoother and larger (2mm diameter, with a hole through the center promoting easier air flow), allowing for greater compliance in both the soft and rigid states, while coffee has been shown to have very sharp particle geometry and therefore is more rigid [26]. Consequently, the coffee filled version does have some dropoff in performance on high curvatures.

D. System Demonstration

Once completed, the true test of the design is how well it works in the real world. To this end, a prototype was mounted on a UR5 robotic arm and used to pick up, manipulate, and place a series of dishes starting in a deep sink and finishing in a dish rack. Figure 12 shows a progression of still shots from this operation, which was a single, continuous manipulation sequence. Video of this procedure is available for download from the IEEE website.

V. Conclusions and Future Work

This work represents an initial exploration of the advantages of increased range of motion at the distal end of a kinematic chain. Hyperextension of the distal phalanges is shown to increase grasp security pinches; hyperextension of proximal phalanges allows for easy transitions between anthropomorphic and suction based grasps, and 180° of available rotation at a bending wrist joint located close to the grasping point results in an extended configuration space and manipulation options. Further, particle jamming

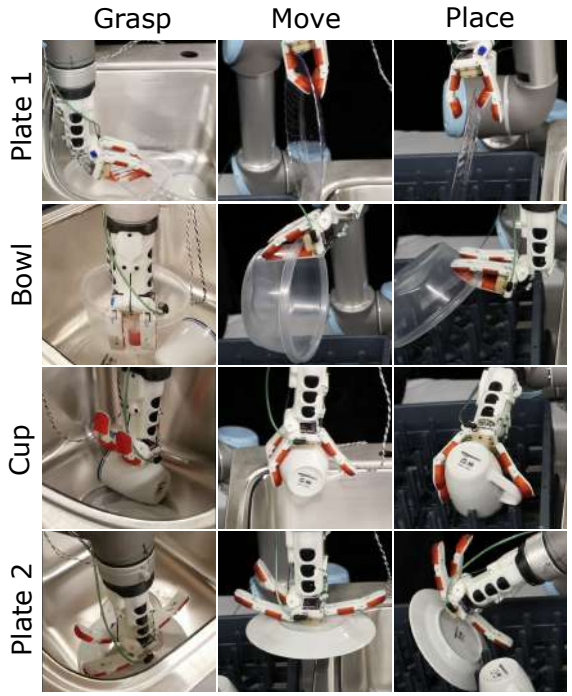

Fig. 12. Selected frames from manipulation demonstration video. Starting at the top left and ending in the bottom right (chronologically) these images show key grasps and movement patterns that were successfully used to pick and place the dishes shown.

substrates are shown to improve the performance of non-aspirated suckers by allowing for both passive conformation to curved surfaces and nearly rigid distribution of force across the contact interface in a single device. Pull out and pull off tests verify these results quantitatively, and a tendon driven, underactuated prototype demonstrates qualitative efficacy in a simulated kitchen environment.

Limitations of the system stem primarily from fabrication limitations. Structures were mostly made using a Formlabs Form 2 printer, and so low motor torques were needed to prevent hardware damage. These low motor torques reduced manipulation speed and limited grasp force, which sometimes prevented the fingers from settling into the desired full planar contact condition. Future prototypes will avoid this difficulty with stronger materials, allowing the motors to be actuated at a higher percentage of their total capacity and thus improve grasp security significantly.

REFERENCES

[1] R. B. Rusu, B. Gerkey, and M. Beetz, "Robots in the kitchen: Exploiting ubiquitous sensing and actuation," *Robotics and Autonomous Systems*, vol. 56, no. 10, pp. 844–856, 2008.

[2] A. Pacheco-Ortega, H. Estrada, E. Vázquez, R. Martell, J. Hernández, J. Cruz, E. Silva, J. Savage, and L. Contreras, "Intelligent flat-and-textureless object manipulation in service robots," *arXiv preprint arXiv:1809.03210*, 2018.

[3] J. Bohg and D. Kragic, "Learning grasping points with shape context," *Robotics and Autonomous Systems*, vol. 58, no. 4, pp. 362–377, 2010.

[4] M. Oleynik, "Methods and systems for food preparation in a robotic cooking kitchen," Nov. 14 2017, uS Patent 9,815,191.

[5] P. M. Birkmeyer, L. H. Pouliot, and K. M. Peters, "Dish manipulation systems and methods," Feb. 8 2018, uS Patent App. 15/665,260.

[6] M. Grebenstein, A. Albu-Schäffer, T. Bahls, M. Chalon, O. Eiberger, W. Friedl, R. Gruber, S. Haddadin, U. Hagn, R. Haslinger *et al.*, "The dlr hand arm system," in *2011 IEEE International Conference on Robotics and Automation*. IEEE, 2011, pp. 3175–3182.

[7] A. Kochan, "Shadow delivers first hand," *Industrial robot: an international journal*, vol. 32, no. 1, pp. 15–16, 2005.

[8] F. Negrello, S. Mghames, G. Grioli, M. Garabini, and M. G. Catalano, "A compact soft articulated parallel wrist for grasping in narrow spaces," *IEEE Robotics and Automation Letters*, vol. 4, no. 4, pp. 3161–3168, 2019.

[9] D. Prattichizzo, M. Malvezzi, M. Gabiccini, and A. Bicchi, "On the manipulability ellipsoids of underactuated robotic hands with compliance," *Robotics and Autonomous Systems*, vol. 60, no. 3, pp. 337–346, 2012.

[10] L. Birglen and C. M. Gosselin, "Kinetostatic analysis of underactuated fingers," *IEEE Transactions on Robotics and Automation*, vol. 20, no. 2, pp. 211–221, 2004.

[11] C. Piazza, G. Grioli, M. Catalano, and A. Bicchi, "A century of robotic hands," *Annual Review of Control, Robotics, and Autonomous Systems*, vol. 2, pp. 1–32, 2019.

[12] F. L. Hammond, J. Weisz, A. Andrés, P. K. Allen, and R. D. Howe, "Towards a design optimization method for reducing the mechanical complexity of underactuated robotic hands," in *2012 IEEE International conference on robotics and automation*. IEEE, 2012, pp. 2843–2850.

[13] M. Ciocarlie and P. Allen, "Data-driven optimization for underactuated robotic hands," in *2010 IEEE International Conference on Robotics and Automation*. IEEE, 2010, pp. 1292–1299.

[14] D. Aukes, B. Heyneman, V. Duchaine, and M. R. Cutkosky, "Varying spring preloads to select grasp strategies in an adaptive hand," *2011 IEEERSJ International Conference on Intelligent Robots and Systems*, pp. 1373–1379, 2011.

[15] R. R. Ma and A. M. Dollar, "Linkage-based analysis and optimization of an underactuated planar manipulator for in-hand manipulation," *Journal of Mechanisms and Robotics*, vol. 6, no. 1, p. 011002, 2014.

[16] L. U. Odhner and A. M. Dollar, "Stable, open-loop precision manipulation with underactuated hands," *The International Journal of Robotics Research*, vol. 34, no. 11, pp. 1347–1360, 2015.

[17] N. Correll, K. E. Bekris, D. Berenson, O. Brock, A. Causo, K. Hauser, K. Okada, A. Rodriguez, J. M. Romano, and P. R. Wurman, "Analysis and observations from the first amazon picking challenge," *IEEE Transactions on Automation Science and Engineering*, vol. 15, no. 1, pp. 172–188, 2016.

[18] S. Hasegawa, K. Wada, Y. Niitani, K. Okada, and M. Inaba, "A three-fingered hand with a suction gripping system for picking various objects in cluttered narrow space," in *2017 IEEE/RSJ International Conference on Intelligent Robots and Systems (IROS)*. IEEE, 2017, pp. 1164–1171.

[19] F. Tramacere, L. Beccai, F. Mattioli, E. Sinibaldi, and B. Mazzolai, "Artificial adhesion mechanisms inspired by octopus suckers," in *2012 IEEE International Conference on Robotics and Automation*. IEEE, 2012, pp. 3846–3851.

[20] T. Tomokazu, S. Kikuchi, M. Suzuki, and S. Aoyagi, "Vacuum gripper imitated octopus sucker-effect of liquid membrane for absorption," in *2015 IEEE/RSJ International Conference on Intelligent Robots and Systems (IROS)*. IEEE, 2015, pp. 2929–2936.

[21] M. R. Cutkosky *et al.*, "On grasp choice, grasp models, and the design of hands for manufacturing tasks." *IEEE Transactions on robotics and automation*, vol. 5, no. 3, pp. 269–279, 1989.

[22] D. Aukes, S. Kim, P. Garcia, A. Edsinger, and M. R. Cutkosky, "Selectively compliant underactuated hand for mobile manipulation," in *2012 IEEE International conference on robotics and automation*. IEEE, 2012, pp. 2824–2829.

[23] D. M. Aukes, B. Heyneman, J. Ulmen, H. Stuart, M. R. Cutkosky, S. Kim, P. Garcia, and A. Edsinger, "Design and testing of a selectively compliant underactuated hand," *The International Journal of Robotics Research*, vol. 33, no. 5, pp. 721–735, 2014.

[24] F. Tramacere, L. Beccai, M. Kuba, A. Gozzi, A. Bifone, and B. Mazzolai, "The morphology and adhesion mechanism of octopus vulgaris suckers," *PLoS One*, vol. 8, no. 6, p. e65074, 2013.

[25] K. Matsuda, D. Hashimoto, and K. Nakamura, "Real contact area and friction property of rubber with two-dimensional regular wavy surface," *Tribology International*, vol. 93, pp. 523–529, 2016.

[26] E. Brown, N. Rodenberg, J. Amend, A. Mozeika, E. Steltz, M. R. Zakin, H. Lipson, and H. M. Jaeger, "Universal robotic gripper based on the jamming of granular material," *Proceedings of the National Academy of Sciences*, vol. 107, no. 44, pp. 18 809–18 814, 2010.